Available online at www.sciencedirect.com

ScienceDirect

Advances in Space Research 68 (2021) 2138–2151

ADVANCES IN SPACE RESEARCH (a COSPAR publication)

www.elsevier.com/locate/asr

Investigating different vTEC calibration methods for data assimilation in ionospheric empirical models

A. Pignalberi [a,*], M. Pietrella [a], M. Pezzopane [a], J.B. Habarulema [b,c]

[a] Istituto Nazionale di Geofisica e Vulcanologia, Via di Vigna Murata 605, 00143 Rome, Italy
[b] South African National Space Agency, Space Science, Hospital St, 7200 Hermanus, South Africa
[c] Department of Physics and Electronics, Rhodes University, Artillery Road, 6140 Grahamstown, South Africa

Received 5 May 2020; received in revised form 27 August 2020; accepted 24 October 2020
Available online 13 November 2020

Abstract

A new data assimilation procedure in the International Reference Ionosphere UPdate (*IRI UP*) method has been recently implemented. This new procedure relies on the assimilation of vertical total electron content (vTEC) values from a Global Navigational Satellite Systems ground-based receivers network, calibrated through the *Seemala*'s method (*IRI UP Seemala*), to obtain an updated description of F2-peak ionospheric characteristics over the South-African region.

The main purpose of this paper is to investigate how the use of different vTEC calibration methods affects the *IRI UP* method. In this work, the *IRI UP* method is applied on periods already analysed in the past (several quiet and disturbed periods in 2017 and 2018), but assimilating vTEC values calibrated through the *Ciraolo*'s method (*IRI UP Ciraolo*). In this way, it is possible to make a homogeneous and fair comparison between results obtained with the two different calibration methods.

Overall, it emerges that *IRI UP Ciraolo* models *fo*F2 with a precision that is always greater than the *IRI UP Seemala*'s one, mainly at nighttime and solar terminator hours, for both quiet and disturbed periods; while slight improvements are achieved during daytime hours. Their accuracy is instead quite similar. Anyhow, the IRI *fo*F2 modeling over the South-African region is significantly improved by both procedures, thus providing a valuable tool to improve IRI model performances.

Keywords: IRI UP method; vTEC data assimilation; vTEC calibration methods; *fo*F2 modeling

1. Introduction

Pignalberi et al. (2019) have recently proposed a new procedure of data assimilation of vertical total electron content (vTEC) values, from ground-based Global Navigational Satellite Systems (GNSS) receivers, in ionospheric empirical climatological models, to get updated F2-layer peak parameters over a given region.

Specifically, in Pignalberi et al. (2019) (hereafter *SWj_paper*) vTEC values obtained from the South-African GNSS network named TrigNet (http://www.trignet.co.za,), were assimilated in the International Reference Ionosphere (IRI, Bilitza et al., 2017) model through the International Reference Ionosphere UPdate (*IRI UP*) method (Pietrella et al., 2018; Pignalberi et al, 2018a,b; Pignalberi, 2019). The proposed methodology turned out to be appropriate for *fo*F2 (the ordinary critical frequency of the F2 layer) modeling, highlighting at the same time the functionality of *IRI UP* method for Space Weather nowcasting purposes when real-time vTEC data are available for assimilation.

* Corresponding author.
E-mail addresses: alessio.pignalberi@ingv.it (A. Pignalberi), marco.pietrella@ingv.it (M. Pietrella), michael.pezzopane@ingv.it (M. Pezzopane), jhabarulema@sansa.org.za (J.B. Habarulema).

https://doi.org/10.1016/j.asr.2020.10.040
0273-1177/

In *SWj_paper*, vTEC calibrated data were derived from TrigNet Receiver INdependent Exchange (RINEX) observation files by using the vTEC calibration software tool available at http://seemala.blogspot.com, developed by the Boston College (Seemala and Valladares, 2011), hereafter indicated as *Seemala*'s calibration method. Thereafter, as a step forward, we investigated the application of different vTEC calibration methods in the *IRI UP* procedure. In particular, we investigated the application of *Ciraolo*'s vTEC calibration method (Ciraolo et al., 2007). As a consequence, we re-calibrated the entire TrigNet GNSS dataset used in *SWj_paper* with the *Ciraolo*'s method, for both the collocated reference stations and assimilated TrigNet GNSS stations.

Therefore, in the present paper, the same methodology and validation adopted in *SWj_paper* is applied with the only difference that vTEC values used in this investigation are calibrated through the *Ciraolo*'s method. Validation is performed for the same time periods investigated in *SWj_paper* (some intense geomagnetic storms in 2017, some quiet periods for different seasons in 2017, and some quiet and disturbed periods in 2018), by focusing on the *fo*F2 ionospheric characteristic. In such a way, a fair comparison between the results obtained using *IRI UP Seemala* (i.e., the results in *SWj_paper*) and the ones obtained by *IRI UP Ciraolo* (i.e., the ones presented in this paper) is possible. In addition, a comparison between *IRI UP Seemala* and *IRI UP Ciraolo* performance for quasi-stationary hours (daytime and nighttime) and non-stationary hours (the ones affected by the solar terminator passage) is performed by selecting three different local time (LT) sectors: daytime [8,16), nighttime [21,5), and combined dawn and dusk hours [5,8) ∪ [16,21). Consider that for the South-African region LT = UT + 2 (UT is the Universal Time).

A case study for the Hermanus (34.42° S, 19.22° E, South Africa) testing station is discussed in detail for the period 1–19 September 2017, including an intense geomagnetic storm. Anyhow, the whole analysis expressed in terms of some key statistical quantities useful to assess the precision and accuracy of both methods is provided as Supplementary Material.

The mathematical relationship between vTEC and *Nm*F2 (the maximum electron density of the F2 layer, related to *fo*F2 through the formula $foF2[\mathrm{MHz}] = (NmF2[\mathrm{el/m^3}]/1.24\mathrm{x}10^{10})^{1/2}$, Davies (1990)) data, along with a brief recall about the data processing introduced in *SWj_paper*, is presented in Section 2. In the same section, a self-validation test of the proposed approach is provided. The validation test for the Hermanus case study for the period 1–19 September 2017 is outlined in Section 3. The description of the Supplementary Material along with some considerations about differences between *IRI UP Ciraolo* and *IRI UP Seemala* performances are the subject of Section 4. Conclusive remarks and possible future developments are outlined in Section 5.

2. Mathematical relationship between vTEC and *Nm*F2 and a brief recall about the data processing

As outlined in the Introduction, in this study the same methodology and validation analysis proposed in *SWj_paper* are considered, focusing on *fo*F2, with the only difference that vTEC time series are now calculated by the *Ciraolo*'s calibration method. For the reader convenience, the dataset creation and the fundamental steps of this methodology are here described; further details can be found in Pignalberi et al. (2019).

The dataset employed in this study, and investigated in *SWj_paper*, consists of ionosondes' derived *Nm*F2 values and vTEC values from ground-based GNSS receivers, both located in the South-African region. Specifically, we consider four South-African ionosondes: Grahamstown (33.30° S, 26.50° E), Hermanus (34.42° S, 19.22° E), Louisvale (28.50° S, 21.20° E), and Madimbo (22.39° S, 30.88° E). These ionospheric stations are equipped with DPS Digisondes (Bibl and Reinisch, 1978), operating routinely with a 15-minutes sounding repetition rate, and providing ionograms that are automatically scaled by the Automatic Real-Time Ionogram Scaler with True height analysis (ARTIST) software (Galkin and Reinisch, 2008). We selected only autoscaled *fo*F2 values whose Confidence Score (C-Score) parameter (see http://www.ursi.org/files/CommissionWebsites/INAG/web-73/confidence_score.pdf) is ≥75. Ionosonde data were downloaded from the Digital Ionogram DataBASE (Reinisch and Galkin, 2011) by means of the SAO Explorer software developed by the University of Massachusetts, Lowell (https://ulcar.uml.edu/SAO-X/SAO-X.html).

vTEC data are obtained through calibration of daily RINEX files, containing L1 and L2 code and carrier phase data at a 30-seconds epoch rate, collected by four ground-based GNSS receivers: Grahamstown (33.30° S, 26.50° E), Hermanus (34.42° S, 19.22° E), Thohoyandou (23.08° S, 30.38° E), and Upington (28.40° S, 21.25° E). Grahamstown and Hermanus GNSS receivers and ionosonde stations are perfectly collocated, while Louisvale and Upington are 12 km apart, Madimbo and Thohoyandou are 92 km apart. These four GNSS receivers are part of the TrigNet network (http://www.trignet.co.za/) consisting in 68 ground-based GNSS stations located throughout South Africa. RINEX files were downloaded at ftp://ftp.trignet.co.za. Both *Seemala*'s (Seemala & Valladares, 2011) and *Ciraolo*'s (Ciraolo et al., 2007) calibration procedures are applied on the dataset of daily RINEX files downloaded from the TrigNet network. For both calibration procedures the equivalent vTEC at the ionospheric pierce point of 350 km is calculated assuming a thin spherical shell model. The cut-off elevation angle is 50° when considering vTEC values used to describe the *Nm*F2 vs vTEC relation over collocated stations (Eq. (1)), while it is 20° for vTEC values that are subsequently assimilated in *IRI UP* (see Section 3). Further details about how vTEC data are obtained, along with a detailed description of the

data processing, are provided in *SWj_paper* in Sections 3.3 and 3.4.

The core of the method is the existence of a strong correlation between vTEC (regardless from how it is calibrated) and *Nm*F2, as pointed out by several authors (e.g., Spalla and Ciraolo, 1994; Kouris et al., 2004; Leitinger et al., 2004; Krankowski et al., 2007; Gerzen et al., 2013; Ssessanga et al., 2014). In *SWj_paper*, the following linear relationship between $\log_{10}$(vTEC) and $\log_{10}(NmF2)$ was used:

$$\log_{10}(NmF2) = a_{NmF2}\log_{10}(\text{vTEC}) + b_{NmF2}. \quad (1)$$

Eq. (1) is applied to the dataset used in this work consisting of collocated and simultaneous *Nm*F2 and vTEC data recorded over the years 2006–2017 at Grahmastown, 2008–2017 at Hermanus, 2004–2017 at Louisvale, and 2003–2017 at Madimbo, at a 15-minutes time rate.

When applied to the entire dataset, a single couple of slope (a_{NmF2}) and intercept (b_{NmF2}) values is obtained through the linear relationship (1). As a consequence, these values represent a mean behaviour irrespective of the hour of the day, season, and year. Density plots of $\log_{10}$(vTEC) vs $\log_{10}(NmF2)$, for the entire dataset, are given in left panels of Fig. 1, for *Seemala*'s vTEC calibration method on top panels, and *Ciraolo*'s vTEC calibration method on bottom panels.

Calculated slope and intercept coefficients are:

- *Seemala*'s calibration method: $a_{NmF2} = 0.925$ and $b_{NmF2} = -4.116$;
- *Ciraolo*'s calibration method: $a_{NmF2} = 0.998$ and $b_{NmF2} = -5.425$.

Then, calculated fitting coefficients a_{NmF2} and b_{NmF2} are put in (1) to calculate modeled *Nm*F2 values which are converted in *fo*F2 modeled values and compared to *fo*F2 values measured by ionosondes.

The root mean square error (RMSE), normalized root mean square error (NRMSE), and Pearson correlation coefficient (R) statistical metrics are also given in Fig. 1:

$$\text{RMSE [MHz]} = \sqrt{\frac{\sum_{i=1}^{N}(foF2_{\text{modeled},i} - foF2_{\text{measured},i})^2}{N}}, \quad (2)$$

$$\text{NRMSE [\%]} = \frac{\text{RMSE}(foF2_{\text{modeled}}, foF2_{\text{measured}})}{\overline{foF2_{\text{measured}}}} \cdot 100, \quad (3)$$

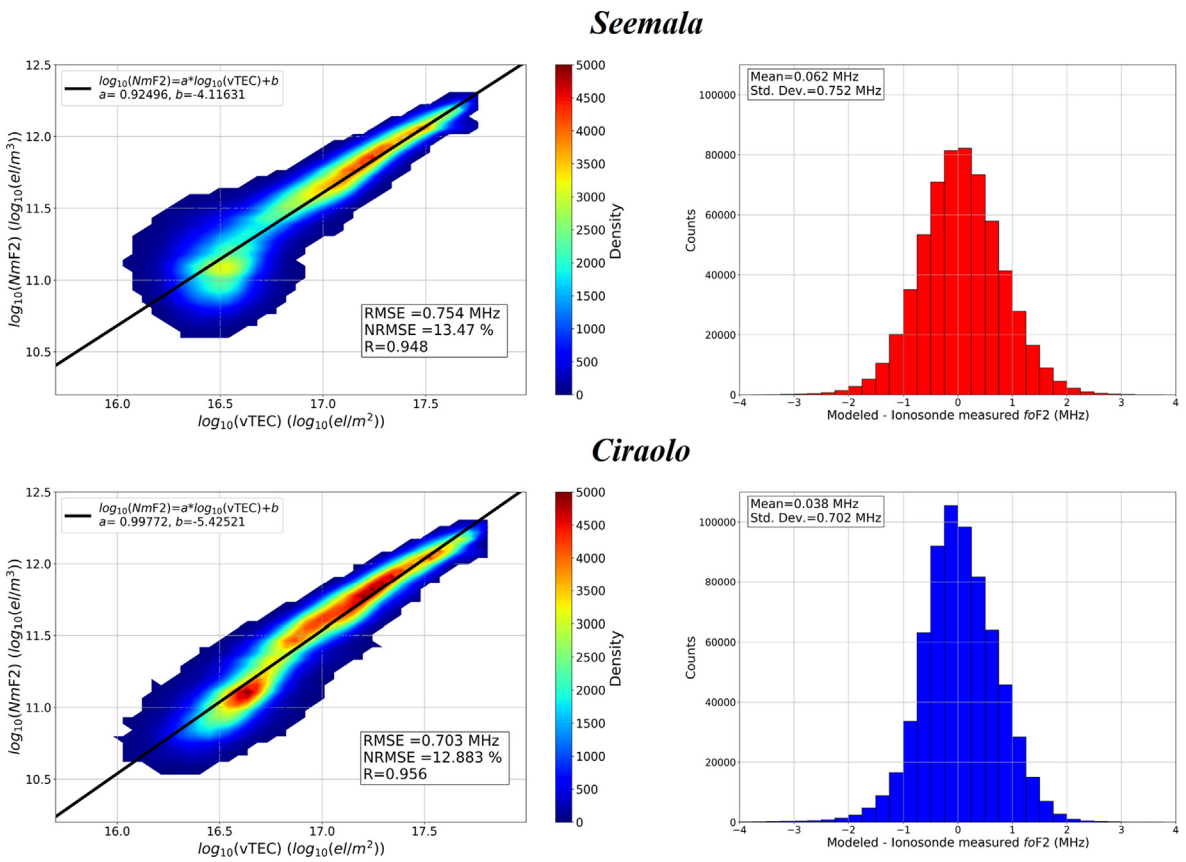

Fig. 1. (left panels) Two-dimensional density plot of $\log_{10}(NmF2)$ vs $\log_{10}$(vTEC) with the corresponding fitting linear function (solid black line). (right panels) Histogram of corresponding residuals between modeled and measured *fo*F2 values. Top panels concern results obtained with *Seemala* calibration method (adapted from Fig. 2 of *SWj_paper*), bottom panels concern results obtained with *Ciraolo* calibration method.

$$R = \frac{\mathrm{cov}(foF2_{\mathrm{modeled}}, foF2_{\mathrm{measured}})}{\sigma_{foF2_{\mathrm{modeled}}}\sigma_{foF2_{\mathrm{measured}}}} \in [-1, 1], \quad (4)$$

where the subscript *modeled* refers to *fo*F2 values obtained through Eq. (1) with fitting coefficients a_{NmF2} and b_{NmF2}, while the subscript *measured* refers to values recorded by ionosondes; the index i runs on the N values of the time series. $\overline{foF2_{\mathrm{measured}}}$ is the arithmetic mean of $foF2_{\mathrm{measured}}$, cov is the covariance between modeled and measured values, and σ the corresponding standard deviation.

Corresponding histograms of residuals between modeled and measured *fo*F2 values are shown in the right panels of Fig. 1, for *Seemala* on top right panel, and *Ciraolo* on bottom right panel. In the same panels, the mean and standard deviation of residuals are reported.

The comparison between results derived by the *Seemala*'s vTEC calibration method (top panels of Fig. 1), and those derived by the *Ciraolo*'s vTEC calibration method (bottom panels of Fig. 1), indicates that the linear fitting procedure turns out to be more accurate when using *Ciraolo*'s calibration method; in fact, the residuals mean calculated for *Seemala* (0.062 MHz) is greater than the one calculated for *Ciraolo* (0.038 MHz). The *Seemala* dispersion around the fitting linear function (Std. Dev. = 0.752 MHz) is slightly greater than the *Ciraolo*'s one (Std. Dev. = 0.702 MHz); in both cases, the dispersion is particularly emphasized in correspondence of small values of *Nm*F2 and vTEC, that is during nighttime hours. The comparison of RMSE (0.754 MHz for *Seemala*, 0.703 MHz for *Ciraolo*), NRMSE (13.470% for *Seemala*, 12.883% for *Ciraolo*), and Pearson correlation coefficient (0.948 for *Seemala*, 0.956 for *Ciraolo*) statistical values, confirms an overall improvement given by the use of *Ciraolo*'s vTEC calibration method.

2.1. Modeling the diurnal and seasonal variability of vTEC vs NmF2 data

To take into account the diurnal and seasonal variation that both *Nm*F2 and vTEC exhibit, *Nm*F2 and corresponding vTEC values collected at the four collocated stations are binned by month (m) and UT hour (h), and the linear relationship (1) is considered for each m and h. Consequently, 288 (12 months × 24 hours) couples of coefficients a_{NmF2} and b_{NmF2} are calculated. Fig. 2 shows the a_{NmF2} and b_{NmF2} coefficients matrices as a function of UT hour (x axis) and month of the year (y axis), for *Seemala*'s (top panels) and *Ciraolo*'s (bottom panels) calibration methods.

From the comparison between matrices of Fig. 2, it emerges that the main differences are related to nighttime and solar terminator hours. The slopes calculated when calibrating vTEC with the *Ciraolo*'s method show values higher than the ones calculated by the *Seemala*'s method at night, while slightly lower values than ones calculated by the *Seemala*'s method are observed during daytime. Vice versa, the intercepts calculated when calibrating vTEC with the *Ciraolo*'s method show values lower than ones calculated by the *Seemala*'s method at night, while no important differences are observed between the two methods during daytime. These differences mean that the two vTEC calibration methods will lead the *IRI UP* method to model *fo*F2 differently, a fact that will be clear in the following sections.

2.2. A first self-validation procedure

The 288 couples of coefficients a_{NmF2} and b_{NmF2} depicted in Fig. 2 are exploited to perform a self-testing of the proposed approach. Specifically, vTEC values recorded at the four collocated GNSS receivers are used to calculate modeled *Nm*F2 values by means of Eq. (1) and coefficients of Fig. 2. *fo*F2 modeled values are then obtained from *Nm*F2 and compared with *fo*F2 measurements recorded at the four collocated ionosonde stations. RMSE, NRMSE, and R values (Eqs. (2)-(4)) are calculated by considering modeled and measured *fo*F2 values, for each bin of Fig. 2. Corresponding results are represented in Fig. 3.

Comparing matrices of Fig. 3, we found that the main differences concern values at nighttime and solar terminator hours. This is particularly evident looking at R values during nighttime and solar terminator hours, for which *Ciraolo*'s values are always higher than *Seemala*'s ones, highlighting an improved correlation. Instead, during daytime R values are very similar. Therefore, this comparison indicates that vTEC values calibrated by the *Ciraolo*'s method can better reproduce the original dataset than the *Seemala*'s one, during nighttime hours and when the solar terminator sets very strong gradients in the electron density, i.e., at dawn and dusk.

The comparison between mean values of the elements of matrices of Fig. 3 for *IRI UP Ciraolo*, $\mathrm{RMSE_{MEAN}} = 0.504$-MHz and $\mathrm{NRMSE_{MEAN}} = 10.513\%$, with the mean values calculated irrespective of the hour of the day and season shown in Fig. 1 namely, RMSE = 0.703 MHz and NRMSE = 12.883%, supports the fact that an important advance is achieved when the hourly and monthly dependence is considered when modeling the vTEC vs *Nm*F2 relationship.

Moreover, the comparison with corresponding results for *Seemala*, $\mathrm{RMSE_{MEAN}} = 0.553$ MHz and $\mathrm{NRMSE_{MEAN}} = 11.662\%$, constitutes a further evidence about the fact that the *fo*F2 modeling is improved when the *Ciraolo*'s vTEC calibration method is used instead of *Seemala*'s one.

3. Assimilation of GNSS-derived vTEC measurements for updating the IRI model and validation of the proposed method

vTEC values coming from the whole Trignet GNSS receivers network are used in the assimilation process, while *fo*F2 data from the four South-African ionosonde

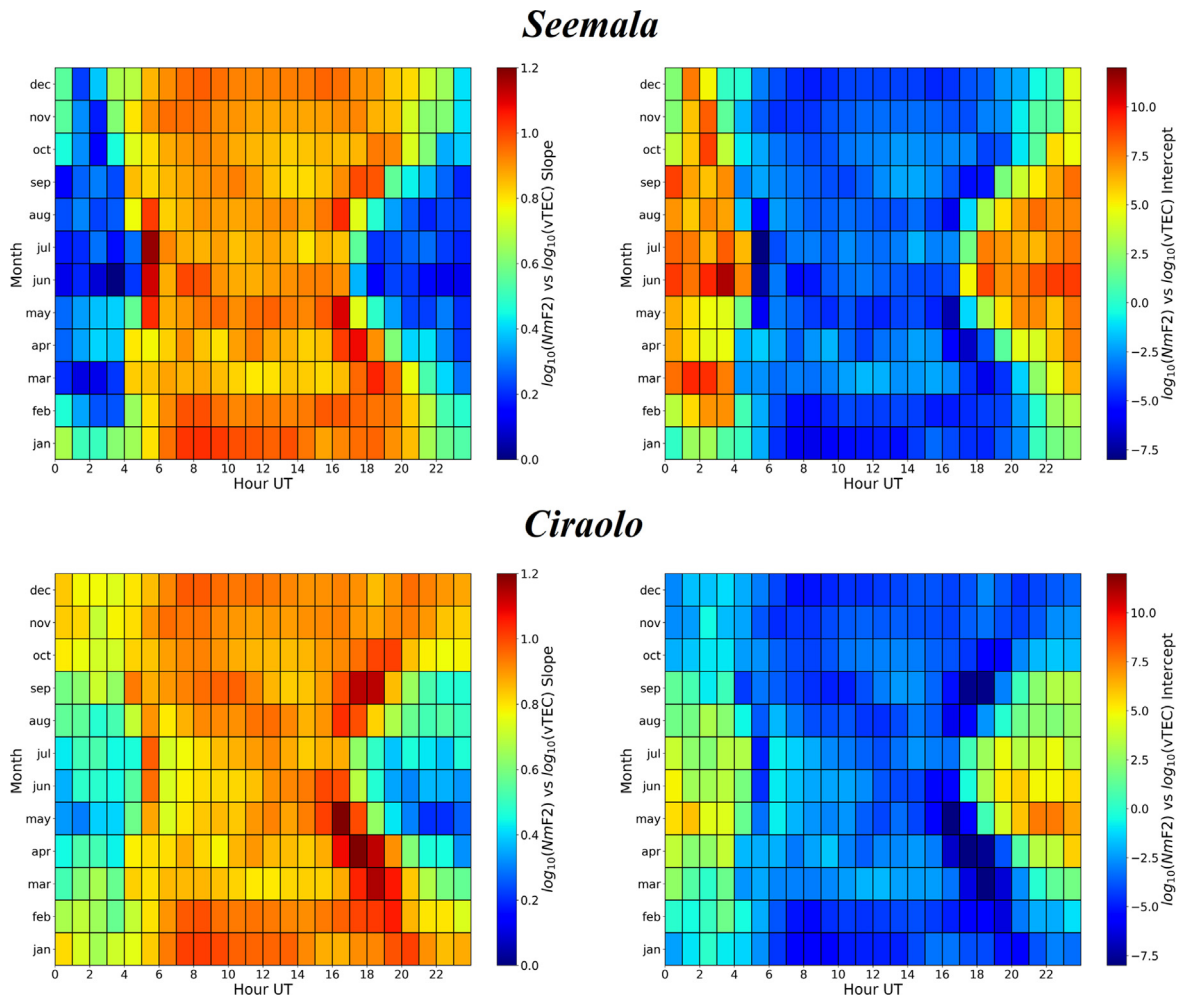

Fig. 2. Matrices of the linear fitting coefficients a_{NmF2} (left panels) and b_{NmF2} (right panels) calculated by means of the linear regression (1) for measurements taken at a specific UT hour (x-axis), for a specific month (y-axis), after applying the *Seemala*'s vTEC calibration (top panels, adapted from Fig. 3 of *SWj_paper*), and the *Ciraolo*'s vTEC calibration (bottom panels).

stations are used to test the performance of the proposed method.

The validation tests are performed on:

(a) different disturbed periods selected in the year 2017 named as: MARCH STORM (24 March – 2 April 2017), MAY STORM (25 May – 5 June 2017), JULY STORM (12–22 July 2017), SEPTEMBER 1 STORM (1–19 September 2017), SEPTEMBER 2 STORM (23 September-7 October 2017), NOVEMBER STORM (2–14 November 2017);
(b) four quite time periods ($Kp < 4$) representing different seasons: i.e., SUMMER (1–4 January 2017), AUTUMN (22–25 March 2017), WINTER (22–25 June 2017), SPRING (23–26 September 2017);
(c) two long periods selected in the year 2018, named as: FIRST 2018 PERIOD (10 August – 20 September 2018), including a rather strong geomagnetic storm (25–30 August 2018), SECOND 2018 PERIOD (20 October-20 November 2018), characterized by a relatively long quiet period (20 October-1 November 2018) followed by a period where slight disturbances can be observed.

For a detailed description of validation periods refers to Section 6 of *SWj_paper*.

We have to point out that while the 2017 dataset has contributed to the calculation of the empirical fitting coefficients represented in Fig. 2 (therefore is not an independent dataset), the 2018 dataset is instead an independent one.

3.1. A validation example: Hermanus case study for SEPTEMBER 1 STORM

In this subsection we want to discuss in detail the outcomes achieved by *IRI UP* when vTEC data calculated by the *Ciraolo*'s and *Seemala*'s calibration method are assimilated, focusing the study on the Hermanus testing station for the SEPTEMBER 1 STORM period. This is the most severe geomagnetic storm which occurred in 2017 and deeply affected the High-Frequency propagation

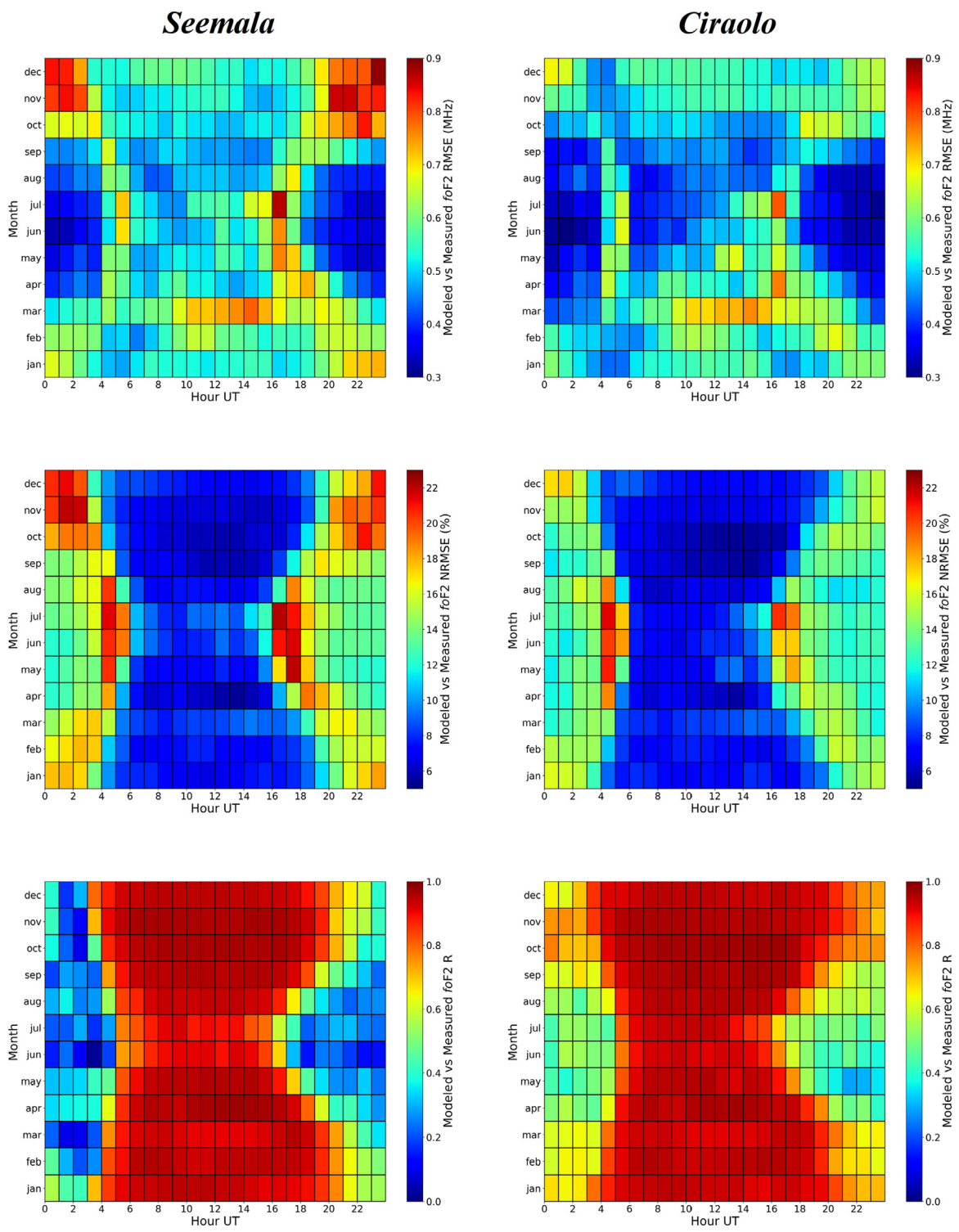

Fig. 3. Matrices of the statistical quantities (top panels) RMSE, (middle panels) NRMSE, and (bottom panels) R between measured and modeled *fo*F2 values depending on the UT hour (*x*-axis) and month (*y*-axis). (left panels) Results obtained applying the *Seemala*'s vTEC calibration method (adapted from Fig. 4 of *SWj_paper*), and (right panels) results obtained applying the *Ciraolo*'s vTEC calibration method.

through the ionosphere (Blagoveshchenskya and Sergeeva, 2019; de Paula et al., 2019; Liu et al., 2020). During the main phase of the storm, on 8 September 2017, the D_{st} index reached a minimum value of −142 nT, while *K*p had a maximum value of 8^{+}. Bottom panels of Figs. 4 and 5 show *K*p and D_{st} geomagnetic indices time series, in black and magenta, respectively. Geomagnetic indices were downloaded from the OMNIWeb Data Explorer NASA site (https://omniweb.gsfc.nasa.gov/form/dx1.html). Orange vertical lines in Figs. 4 and 5 define the quiet

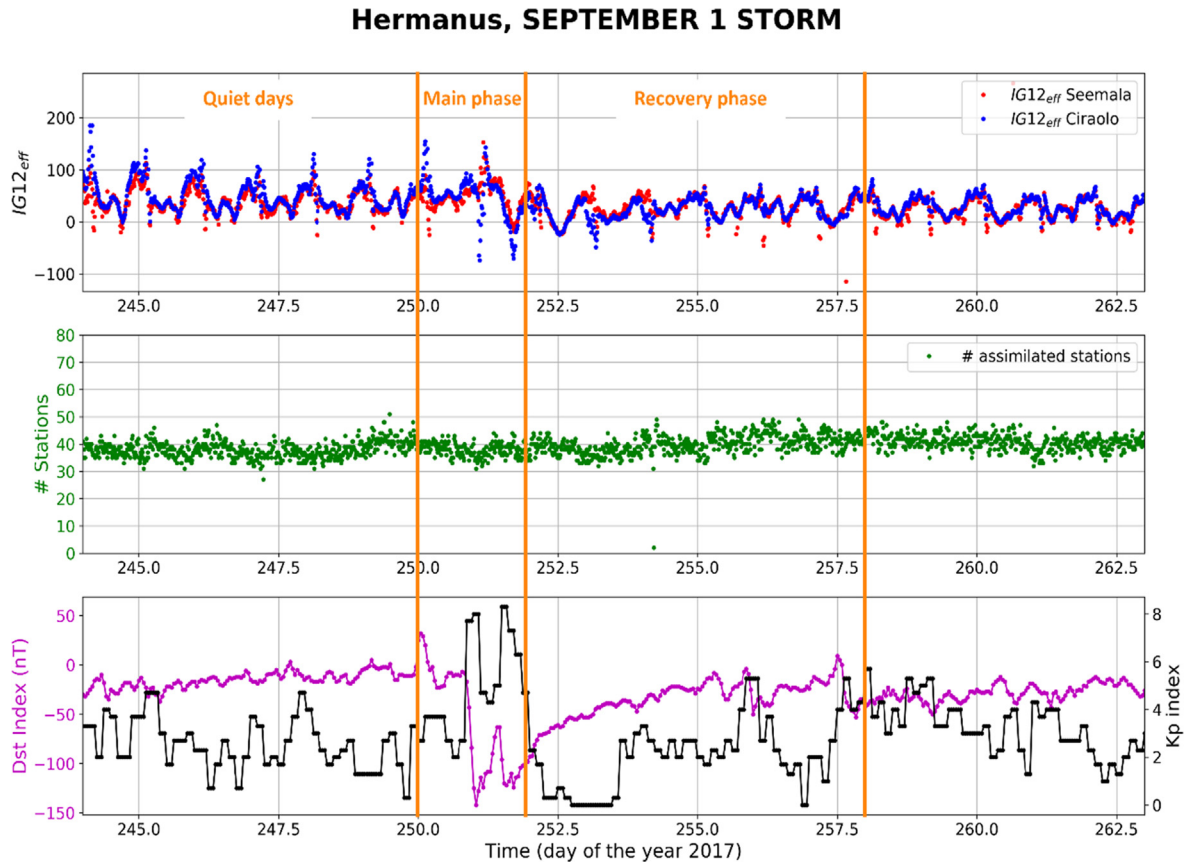

Fig. 4. (top panel) $IG_{12\text{eff}}$ time series derived from (red dots) *Seemala* and (blue dots) *Ciraolo* vTEC calibration method for the period 1–19 September 2017 at Hermanus testing station. (middle panel) Number of assimilated TrigNet GNSS receivers. (bottom panel) *K*p and D_{st} geomagnetic indices time series, in black and magenta, respectively. Orange vertical lines define the quiet, main phase, and recovery phase time windows. (For interpretation of the references to colour in this figure legend, the reader is referred to the web version of this article.)

(1–6 September 2017), main phase (7–8 September 2017), and recovery phase (9–15 September 2017) time windows. It is worth highlighting that the quiet days before the sudden storm commencement (on 7 September 2017), are characterized by *K*p values between 1 and 4, thus they are not completely quiet.

The application of the *IRI UP* method (Pignalberi et al., 2018a, 2018b; Pignalberi, 2019), based on the assimilation of vTEC data obtained with the *Seemala*'s calibration method (*IRI UP Seemala*) and the *Ciraolo*'s calibration method (*IRI UP Ciraolo*), is here briefly described for the benefit of the reader to better comprehend the performed data analysis and corresponding results. The interested reader can find further details in Pignalberi et al. (2019).

According to the procedure described in Section 2.1, the assimilation from TrigNet GNSS stations of vTEC values, calibrated with the *Seemala*'s and *Ciraolo*'s method at a given time t^*, leads to two different datasets of *fo*F2 values calculated for each assimilated GNSS station, one relative to the *Seemala* calibration and the other one relative to the *Ciraolo* calibration.

These *fo*F2 values can be considered as recorded from "virtual" ionosondes collocated with GNSS receivers, and are used to calculate, for each assimilated station, a value of $IG_{12\text{eff}}$, the effective value of the ionospheric index IG_{12} (the 12-months running mean of the ionospheric activity index *IG*, Liu et al., 1983), following the methodology developed by Pignalberi et al. (2018a). Specifically, the squared difference between observed and modeled *fo*F2 values is calculated, for every assimilated station, according to the formula:

$$\Delta_{IG_{12}} = (foF2_{\text{obs}} - foF2_{\text{IRI}}(IG_{12}))^2, \tag{5}$$

where $foF2_{\text{obs}}$ is the value obtained through the application of Eq. (1) and fitting coefficients of Fig. 2 to the assimilated vTEC value, while $foF2_{\text{IRI}}(IG_{12})$ are the corresponding values modeled by IRI as a function of IG_{12}. The effective value of IG_{12}, named $IG_{12\text{eff}}$, is the one minimizing Eq. (5) (Pignalberi et al., 2018a; Pignalberi, 2019). In a nutshell, $IG_{12\text{eff}}$ is the value using which IRI reproduces exactly the assimilated "virtual" *fo*F2 value over the assimilated station at the specific time of assimilation.

Therefore, two $IG_{12\text{eff}}$ sets are calculated at time t^*, one relative to *Seemala* and the other one to *Ciraolo*. The Universal Kriging Method (Kitanidis, 1997) is then applied on these two grids of $IG_{12\text{eff}}$ values to obtain corresponding maps over South Africa at time t^*. These two $IG_{12\text{eff}}$ maps

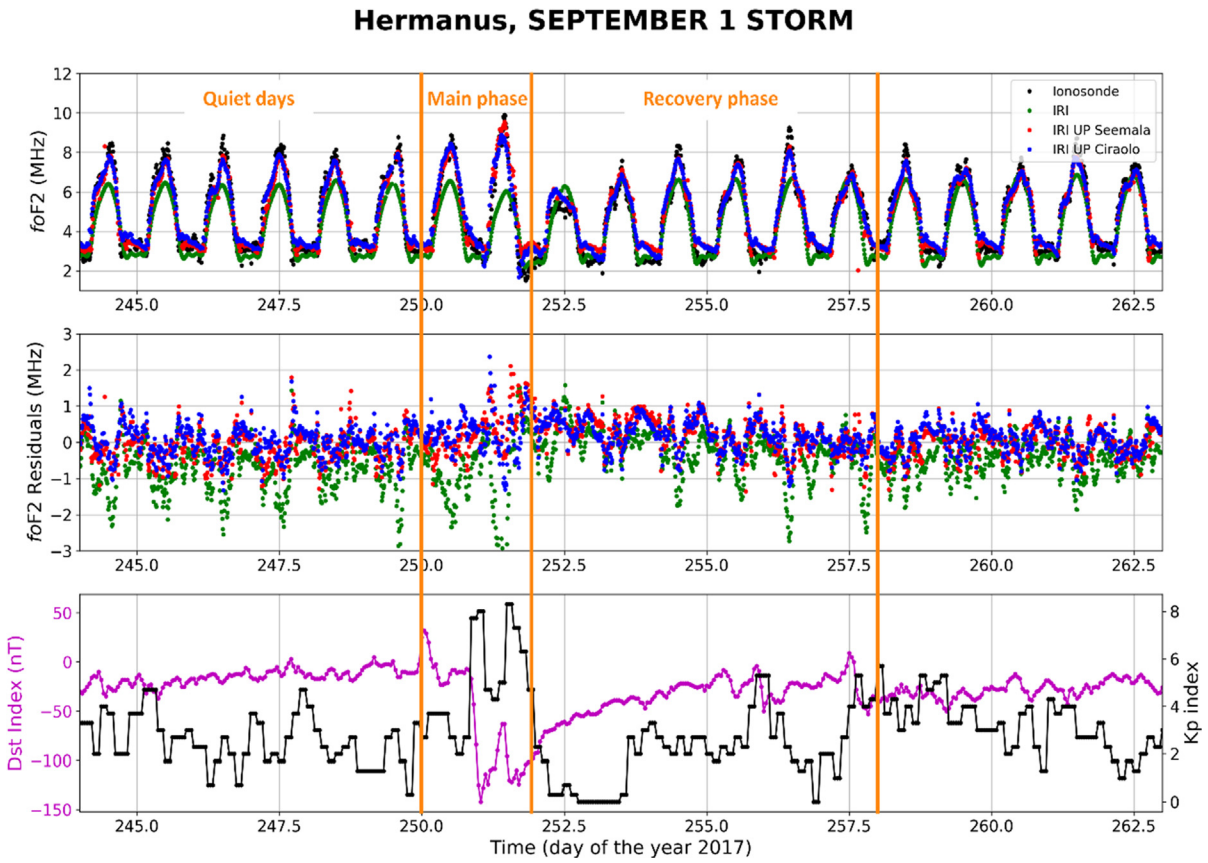

Fig. 5. (top panel) *fo*F2 time series measured by (black dots) Hermanus ionosonde, (green dots) modeled by IRI, (red dots) modeled by *IRI UP Seemala*, and (blue dots) modeled by *IRI UP Ciraolo* for the period 1–19 September 2017. (middle panel) Corresponding time series of residuals between modeled and measured *fo*F2 values. (bottom panel) *K*p and D_{st} geomagnetic indices time series, in black and magenta, respectively. Orange vertical lines define the quiet, main phase, and recovery phase time windows. (For interpretation of the references to colour in this figure legend, the reader is referred to the web version of this article.)

are then used to update the IRI background ionospheric model (Pignalberi et al., 2018a; Pignalberi, 2019; Pignalberi et al., 2019), thus obtaining two maps of *fo*F2 modeled values at time *t**: the *IRI UP Seemala* *fo*F2 modeled values and the *IRI UP Ciraolo* *fo*F2 modeled values.

This approach is validated by comparing *IRI UP Seemala*, *IRI UP Ciraolo*, and IRI (IRI 2016 version, with the STORM option active) *fo*F2 modeled values, with *fo*F2 measurements recorded at the ionosonde testing stations of Grahamstown, Hermanus, Louisvale, and Madimbo, for all the aforementioned testing periods. Obviously, it is not possible to show in the paper the whole amount of analyses done; the interested reader is invited to refer also to the Supplementary Material described in Section 4. Therefore, as a case study, we show and discuss in detail the results achieved at the Hermanus testing station for the period SEPTEMBER 1 STORM (1–19 September 2017).

The top panel of Fig. 4 shows the IG_{12eff} time series calculated at the Hermanus testing station, for the period 1–19 September 2017, generated by applying the *Seemala*'s and *Ciraolo*'s vTEC calibration methods; while the middle panel shows the number of assimilated TrigNet GNSS stations at any time, which depends on the number of available GNSS receivers and on the quality of retrieved vTEC values (for details see *SWj_paper*).

Fig. 5 shows the comparison between *fo*F2 time series modeled by *IRI UP Ciraolo*, *IRI UP Seemala*, and IRI with *fo*F2 time series recorded by the Hermanus ionosonde, along with the corresponding time series of residuals between modeled and measured values.

From a quick visual inspection of Fig. 5, it clearly emerges that during the quiet period (1–6 September 2017), during the main phase (7–8 September 2017) and the recovery phase (9–15 September 2017) of the storm, and for the days after the storm (16–19 September 2017), the IRI model provides the lowest performance by constantly underestimating *fo*F2. It is more difficult to establish whether *IRI UP Ciraolo* prevails on *IRI UP Seemala*, or vice versa.

To this regard, we can rely on the statistical results presented in Fig. 6 showing the histograms of residuals between modeled and measured *fo*F2 values and the corresponding scatterplots, for the whole period 1–19 September 2017. In particular, the *IRI UP Seemala* method turns out to be slightly more accurate than the *IRI UP Ciraolo*'s one,

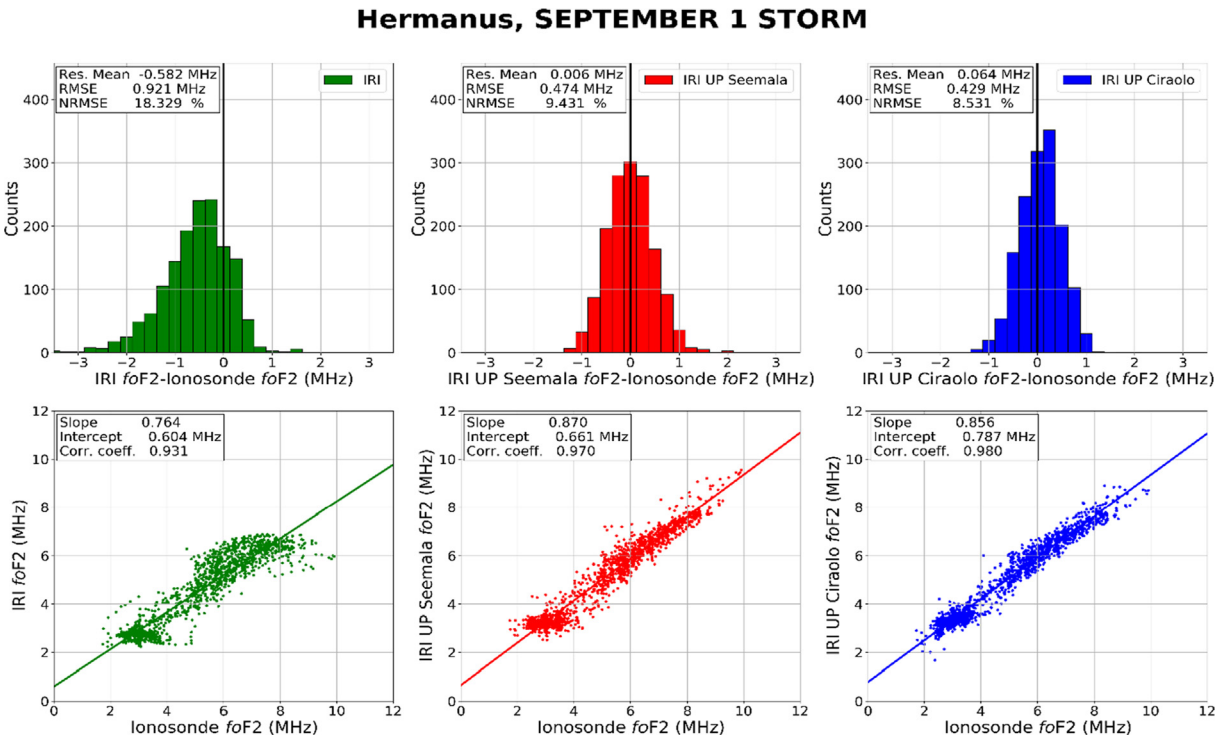

Fig. 6. (top panels) Histograms of residuals shown in the middle panel of Fig. 5, for (green) IRI, (red) *IRI UP Seemala*, and (blue) *IRI UP Ciraolo*, for the period 1–19 September 2017 at Hermanus testing station. The residuals mean, RMSE, and NRMSE values are shown in the upper left corner of each histogram. (bottom panels) Corresponding scatterplots of modeled and measured *fo*F2 values for IRI, *IRI UP Seemala*, and *IRI UP Ciraolo*; straight solid lines are the best fitting linear functions whose slope and intercept values are shown in the upper left corner of each scatterplot, along with the Pearson correlation coefficient. (For interpretation of the references to colour in this figure legend, the reader is referred to the web version of this article.)

being the *Seemala*'s residuals mean (0.006 MHz) smaller than the *IRI UP Ciraolo*'s one (0.064 MHz). Nevertheless, both RMSE and NRMSE are lower for *IRI UP Ciraolo* than for *IRI UP Seemala*, and the *Ciraolo* scatterplot is less scattered than the *Seemala*'s one; this highlights an improvement of the *fo*F2 modeling precision in favour of *IRI UP Ciraolo*.

Statistical values obtained by considering the different phases of the storm are provided in Table 1. Table 1 highlights that *IRI UP Seemala* residuals mean is slightly smaller than the *IRI UP Ciraolo*'s one, for both the main and the recovery phase of the storm. Therefore, *IRI UP Seemala* seems to model *fo*F2 more accurately (mean of residuals closer to zero) than *IRI UP Ciraolo* under disturbed

Table 1
Statistical results for Hermanus, for quiet days before the storm commencement (1–6 September 2017), for the main phase (7–8 September 2017), and the recovery phase (9–15 September 2017) of the SEPTEMBER 1 STORM, and for the whole period (1–19 September 2017). Best statistical results are bolded.

STATION	Model & Characteristic	RMSE [MHz]	NRMSE [%]	R	Residuals mean [MHz]
SEPTEMBER 1 STORM, Quiet days 1–6 September 2017					
Hermanus	IRI *fo*F2	1.049	19.917	0.963	−0.833
	IRI UP *fo*F2 - Seemala	0.457	8.678	0.979	−0.186
	IRI UP *fo*F2 - Ciraolo	**0.404**	**7.672**	**0.985**	**−0.056**
SEPTEMBER 1 STORM, Main Phase days 7–8 September 2017					
Hermanus	IRI *fo*F2	1.515	28.553	0.911	−0.990
	IRI UP *fo*F2 - Seemala	0.627	11.817	0.966	**0.188**
	IRI UP *fo*F2 - Ciraolo	**0.537**	**10.124**	**0.978**	0.193
SEPTEMBER 1 STORM, Recovery Phase days 9–15 September 2017					
Hermanus	IRI *fo*F2	0.719	15.399	0.934	−0.356
	IRI UP *fo*F2 - Seemala	0.485	10.387	0.966	**0.132**
	IRI UP *fo*F2 - Ciraolo	**0.447**	**9.580**	**0.976**	0.156
SEPTEMBER 1 STORM, Full period 1–19 September 2017					
Hermanus	IRI *fo*F2	0.921	18.329	0.931	−0.582
	IRI UP *fo*F2 - Seemala	0.474	9.431	0.970	**0.006**
	IRI UP *fo*F2 - Ciraolo	**0.429**	**8.531**	**0.980**	0.064

geomagnetic conditions. The results of Table 1 also show that *IRI UP Ciraolo* performs better than *IRI UP Seemala* in terms of RMSE, NRMSE, and R for both quiet and disturbed geomagnetic conditions, which indicates a greater precision (lower dispersion around mean) of *IRI UP Ciraolo* in the *fo*F2 modeling. Anyhow, both of them significantly improve IRI performances for both quiet and disturbed periods.

For what concerns the statistical results presented in Table 1, the reader may find slightly different values than those published in *SWj_paper* for what concerns IRI and *IRI UP Seemala*, because the number of values on which the statistics is calculated is slightly different. This is due to a combination of the following reasons (sorted by importance):

1. When calculating the statistics, outliers from test ionosondes were filtered; then, modeled values for such cases are not included in the statistics. In *SWj paper*, this filtering was done simultaneously for both *fo*F2 and *hm*F2 parameters. In this investigation, only *fo*F2 outliers were filtered. This means that, in the present study, the number of points considered by the statistics may be slightly greater than the one considered in *SWj paper*. This happens particularly under disturbed conditions when sometimes the ARTIST system can fail in successfully autoscaling the ionogram;
2. When performing the statistical analysis, modeled *fo*F2 values are discarded when assimilated TrigNet GNSS receivers are less than 9. The unavailability of TrigNet GNSS stations, at a specific time, can depend also on the calibration method. In general, we saw that *Ciraolo*'s vTEC calibration method usually has a greater percentage of success than *Seemala*'s one in calibrating RINEX files;
3. The IRI *fo*F2 output depends on IG_{12} values that are read from the file ig_rz.dat (downloadable at http://irimodel.org/indices/). This file is updated quarterly and the most recent IG_{12} values may vary. Because in this study we consider recent periods, IG_{12} values used in this validation phase have changed with respect to the ones considered in the statistics of *SWj_paper*. Values of IRI *fo*F2 shown in this paper were obtained by using exclusively measured IG_{12} values and not predicted values of IG_{12}, as it was the case of the analysis done in *SWj_paper*.

3.2. Validation for nighttime, daytime and solar terminator hours

Looking at Fig. 3, it is clear that the performance of both models exhibits a different behavior according to the hour of the day. In particular, nighttime and solar terminator hours are affected by larger errors than daytime hours. This is why we decided to investigate the *IRI UP Ciraolo* and *IRI UP Seemala* performance for different LT sectors. Specifically, three different local time sectors are considered:

- daytime: [8,16) LT;
- nighttime: [21,5) LT;
- dawn and dusk (solar terminator hours joined together): [5,8) ∪ [16,21) LT.

Dawn and dusk hours are joined together in a single statistics because the main goal here is to show the different behavior of *IRI UP Seemala* and *IRI UP Ciraolo* during non-stationary conditions (the ones related to the solar terminator passage) compared to quasi-stationary conditions (daytime and nighttime hours). Obviously, we separated daytime and nighttime hours due to the very different correlation between *Nm*F2 and vTEC for those hours (see the bottom panels of Fig. 3). Each subset (daytime, nighttime, and dawn and dusk) is eight hours wide, so it underwent a homogeneous sampling. This kind of analysis represents a novelty with respect to that shown in *SWj_paper*.

Table 2 shows the IRI, *IRI UP Ciraolo* and *IRI UP Seemala* performance for Hermanus testing station, for SEPTEMBER 1 STORM, corresponding to the three different LT sectors just defined.

Results of Table 2 highlight how the assimilation of vTEC data calibrated by *Ciraolo* improves the *IRI UP* performance in terms of RMSE, NRMSE, and R for both daytime and nighttime, and particularly at solar terminator hours. Vice versa, the assimilation of vTEC data calibrated by *Seemala* can slightly improve *IRI UP* performance in terms of residuals mean at nighttime and solar terminator hours. Both calibration methods improve significantly IRI performances during daytime and solar terminator hours, while slight improvements are achieved at nighttime. Preliminary insights given by the self-validation procedure of Section 2.2 are here fully confirmed. Obviously, the Hermanus case study is not sufficient to clarify definitively the differences between *IRI UP Ciraolo* and *IRI UP Seemala*. To this regard, the reader has to refer to the results of Supplementary Material, whose description is provided in Section 4.

4. Overall comparison between *IRI UP Seemala* and *IRI UP Ciraolo*

As already mentioned in the Section 3.1, the whole statistical analysis is provided as Supplementary Material.

Specifically, the Supplementary Material includes:

(a) Figures showing $IG_{12\text{eff}}$ time series derived from the *Seemala*'s and *Ciraolo*'s vTEC calibration methods, the number of assimilated TrigNet GNSS stations, *Kp* and D_{st} geomagnetic indices time series, with the same layout of Fig. 4;
(b) Figures showing measured and modeled *fo*F2 time series and corresponding residuals time series, with the same layout of Fig. 5;

Table 2
Statistical results for Hermanus, during daytime, nighttime, and dawn and dusk hours, for the period 1–19 September 2017. Best statistical results are bolded.

STATION	Model & Characteristic	RMSE [MHz]	NRMSE [%]	R	Residuals mean [MHz]
SEPTEMBER 1 STORM, Full period 1–19 September 2017, Daytime - [8,16) LT					
Hermanus	IRI *fo*F2	1.202	17.437	0.499	−0.830
	IRI UP *fo*F2 - Seemala	0.473	6.855	0.897	−0.135
	IRI UP *fo*F2 - Ciraolo	**0.440**	**6.387**	**0.925**	**−0.127**
SEPTEMBER 1 STORM, Full period 1–19 September 2017, Nighttime - [21,5) LT					
Hermanus	IRI *fo*F2	0.505	16.706	0.006	−0.321
	IRI UP *fo*F2 - Seemala	0.421	13.933	0.363	**0.238**
	IRI UP *fo*F2 - Ciraolo	**0.415**	**13.743**	**0.598**	0.287
SEPTEMBER 1 STORM, Full period 1–19 September 2017, Dawn and Dusk - [5,8) ∪ [16,21) LT					
Hermanus	IRI *fo*F2	0.832	17.842	0.869	−0.530
	IRI UP *fo*F2 - Seemala	0.517	11.088	0.916	**−0.038**
	IRI UP *fo*F2 - Ciraolo	**0.427**	**9.151**	**0.949**	0.086

(c) Figures showing histograms of residuals and corresponding scatterplots, with the same layout of Fig. 6;
(d) Statistical results expressed in terms of RMSE, NRMSE, R, and residuals mean, as in Tables 1 and 2.

Figures and Tables are provided for the four ionosonde testing stations, i.e., Grahamstown, Hermanus, Louisvale, and Madimbo, for all periods listed in Section 3, for the LT sectors [0,24), [8,16), [21,5), and [5,8) ∪ [16,21). The reader can easily access to whatever case, being the Supplementary Material organized in folders whose names reflect the validation periods considered, each of them containing sub-folders for the different LT sectors analysed, *full_dataset* = [0,24), *daytime* = [8,16), *nighttime* = [21,5), and *dawn_and_dusk* = [5,8) ∪ [16,21).

4.1. Main outcomes from statistics on every selected period in 2017 and 2018

From a careful inspection of results of the Supplementary Material, we deduce that *IRI UP Ciraolo* performs by far better than *IRI UP Seemala* in terms of RMSE, NRMSE, and R for each considered LT sector. The higher correlation coefficients R observed almost always in favour of *Ciraolo* are the mathematical proof that *IRI UP Ciraolo* scatterplots are less spread than *IRI UP Seemala*'s ones as, on the other hand, it can be easily verifiable by checking all generated scatterplots. NRMSE values are systematically lower when passing from *IRI UP Seemala* to *IRI UP Ciraolo*. Therefore, we can surely claim that *fo*F2 is modeled with a greater precision by using the *IRI UP Ciraolo* method.

However, it must be pointed out that there are some cases for nighttime hours where IRI performs better than *IRI UP*. This is generally due to the lower correlation between *Nm*F2 and vTEC during nighttime hours, when the plasmasphere contribution becomes more relevant than that of the F2 ionospheric region (Klimenko et al., 2015). Moreover, another reason for which the correlation between *Nm*F2 and vTEC "weakens", so that the IRI model might prevail on *IRI UP*, is the possibility that, particularly under disturbed conditions, the bottomside and topside are no more "linked", being affected by different physical processes (Chi et al., 2000; Förster and Jakowski, 2000; Pezzopane et al., 2019).

On the contrary, if we look at the statistical results concerning the residuals mean it is not easy to draw straight conclusions about the accuracy of the two methodologies, being very similar for most cases.

4.2. Overall outcomes from statistics considering periods in 2017 and 2018 as a joined single dataset

In order to shed light as better as possible on the differences between *IRI UP Ciraolo* and *IRI UP Seemala*, the validation periods mentioned in Section 3 are joined to carry out an overall statistics for each testing station and for the LT sectors [0,24), [8,16), [21,5), and [5,8) ∪ [16,21). Corresponding figures and tables are provided in the Supplementary Material. Here we focus on main outcomes.

Table 3 summarizes statistical results obtained for each testing station joining all validation periods listed in Section 3.

NRMSE results of Table 3 show that *IRI UP Ciraolo* improves *IRI UP Seemala*. In particular, improvements ranging between 3.940% – 11.743% and 2.491% – 3.515% are observed at nighttime and at solar terminator hours, respectively. A slight improvement ranging between 0.601% – 1.959% is obtained during daytime. These results were expected because they faithfully reflect the comparison between matrices of Fig. 3, showing RMSE, NRMSE, and R values clearly in favour of *IRI UP Ciraolo* mainly during nighttime and at solar terminator hours.

Moreover, greater correlation coefficients are observed in favour of *IRI UP Ciraolo* for each testing station and for the four considered LT sectors. Consequently, the *IRI UP Ciraolo* scatterplots are always less scattered than the *IRI UP Seemala's* ones. In the light of these considerations, we can assert that these results provide a further confirma-

Table 3
Statistical results obtained joining all validation periods in 2017 and 2018 as a single dataset, for Grahamstown, Hermanus, Louisvale, and Madimbo testing stations. Best statistical results are bolded.

STATION	Model & Characteristic	RMSE [MHz]	NRMSE [%]	R	Residuals mean [MHz]
ALL PERIODS IN 2017 AND 2018, Full dataset - [0,24) LT					
Grahamstown	IRI *fo*F2	0.732	16.047	0.905	−0.200
	IRI UP *fo*F2 -Seemala	0.511	11.196	0.956	0.169
	IRI UP *fo*F2 –Ciraolo	**0.408**	**8.938**	**0.969**	**0.051**
Hermanus	IRI *fo*F2	0.702	15.226	0.909	−0.137
	IRI UP *fo*F2 -Seemala	0.499	10.819	0.961	0.164
	IRI UP *fo*F2 -Ciraolo	**0.407**	**8.840**	**0.975**	**0.142**
Louisvale	IRI *fo*F2	0.730	16.163	0.909	−0.186
	IRI UP *fo*F2 -Seemala	0.564	12.490	0.943	**0.094**
	IRI UP *fo*F2 -Ciraolo	**0.424**	**9.383**	**0.971**	0.127
Madimbo	IRI *fo*F2	0.780	15.731	0.910	−0.103
	IRI UP *fo*F2 -Seemala	0.696	14.040	0.930	0.109
	IRI UP *fo*F2 -Ciraolo	**0.508**	**10.234**	**0.962**	**−0.010**
ALL PERIODS IN 2017 AND 2018, Daytime - [8,16) LT					
Grahamstown	IRI *fo*F2	0.843	13.877	0.630	−0.119
	IRI UP *fo*F2 -Seemala	0.489	8.055	0.894	0.075
	IRI UP *fo*F2 -Ciraolo	**0.453**	**7.454**	**0.910**	**0.032**
Hermanus	IRI *fo*F2	0.801	13.228	0.676	−0.118
	IRI UP *fo*F2 -Seemala	0.436	7.203	0.916	**0.018**
	IRI UP *fo*F2 -Ciraolo	**0.391**	**6.455**	**0.936**	0.026
Louisvale	IRI *fo*F2	0.843	13.830	0.606	**0.017**
	IRI UP *fo*F2 -Seemala	0.561	9.193	0.842	−0.045
	IRI UP *fo*F2 -Ciraolo	**0.441**	**7.234**	**0.911**	0.040
Madimbo	IRI *fo*F2	0.875	13.403	0.584	**−0.041**
	IRI UP *fo*F2 -Seemala	0.608	9.309	0.825	−0.180
	IRI UP *fo*F2 -Ciraolo	**0.557**	**8.539**	**0.847**	−0.105
ALL PERIODS IN 2017 AND 2018, Nighttime - [21,5) LT					
Grahamstown	IRI *fo*F2	0.598	19.440	0.427	−0.367
	IRI UP *fo*F2 -Seemala	0.505	16.407	0.645	0.280
	IRI UP *fo*F2 -Ciraolo	**0.347**	**11.265**	**0.775**	**0.105**
Hermanus	IRI *fo*F2	0.457	15.281	0.533	**−0.136**
	IRI UP *fo*F2 -Seemala	0.519	17.348	0.726	0.355
	IRI UP *fo*F2 -Ciraolo	**0.401**	**13.408**	**0.826**	0.265
Louisvale	IRI *fo*F2	0.542	17.665	0.487	−0.309
	IRI UP *fo*F2 -Seemala	0.525	17.100	0.616	0.284
	IRI UP *fo*F2 -Ciraolo	**0.376**	**12.256**	**0.805**	**0.211**
Madimbo	IRI *fo*F2	0.621	19.511	0.642	**−0.131**
	IRI UP *fo*F2 -Seemala	0.808	25.366	0.615	0.505
	IRI UP *fo*F2 -Ciraolo	**0.434**	**13.623**	**0.804**	0.190
ALL PERIODS IN 2017 AND 2018, Dawn and Dusk - [5,8) ∪ [16,21) LT					
Grahamstown	IRI *fo*F2	0.725	16.451	0.856	−0.112
	IRI UP *fo*F2 -Seemala	0.542	12.283	0.926	0.157
	IRI UP *fo*F2 -Ciraolo	**0.414**	**9.391**	**0.954**	**0.016**
Hermanus	IRI *fo*F2	0.769	17.075	0.841	−0.161
	IRI UP *fo*F2 -Seemala	0.543	12.061	0.928	**0.149**
	IRI UP *fo*F2 -Ciraolo	**0.431**	**9.570**	**0.960**	0.156
Louisvale	IRI *fo*F2	0.788	17.752	0.860	−0.274
	IRI UP *fo*F2 -Seemala	0.614	13.835	0.905	**0.020**
	IRI UP *fo*F2 -Ciraolo	**0.458**	**10.320**	**0.954**	0.126
Madimbo	IRI *fo*F2	0.820	16.108	0.879	−0.146
	IRI UP *fo*F2 -Seemala	0.659	12.952	0.918	**0.009**
	IRI UP *fo*F2 -Ciraolo	**0.522**	**10.256**	**0.954**	−0.121

tion that *IRI UP Ciraolo* method is, in terms of precision, superior to the *IRI UP Seemala*'s one in modeling *fo*F2.

The main features emerging from the comparison between *IRI UP Seemala* and *IRI UP Ciraolo* residuals mean are:

(a) for the LT sector [0,24), i.e., for the entire day, *IRI UP Ciraolo* performs better than *IRI UP Seemala* except for Louisvale; however, in this case the *IRI UP Seemala - IRI UP Ciraolo* difference (-0.033 MHz) is not significant;

(b) for the LT sector [8,16), *IRI UP Ciraolo* performs slightly better than *IRI UP Seemala* except for Hermanus, but in this case the *Seemala-Ciraolo* difference (-0.008 MHz) is negligible. As a consequence, we can say that the *fo*F2 modeling accuracy of *IRI UP Seemala* and *IRI UP Ciraolo* during daytime is comparable;
(c) for the LT sector [21,5), the situation is sharply in favour of *IRI UP Ciraolo* with the main *Seemala-Ciraolo* differences observed at Grahamstown (+0.175 MHz) and Madimbo (+0.315 MHz). We can therefore claim that for nighttime hours *IRI UP Ciraolo* models *fo*F2 by far more accurately than *IRI UP Seemala*;
(d) for the LT sectors [5,8) ∪ [16,21), *IRI UP Seemala* performs better than *IRI UP Ciraolo* except for Grahamstown. In particular, the main *Seemala-Ciraolo* differences are observed at Louisvale (-0.106 MHz) and Madimbo (-0.112 MHz). Therefore, we can assert that for solar terminator hours *IRI UP Seemala* models *fo*F2 with greater accuracy than *IRI UP Ciraolo*.

It is worth noting that residuals mean exhibited by IRI model are, in some cases, comparable to those exhibited by both *IRI UP* implementations. This is a confirmation that IRI model is very accurate in describing the *fo*F2 variability when considering very long time series (Arıkan et al., 2019). Nevertheless, very important improvements can be achieved concerning the precision (i.e., the dispersion) and the correlation (connected to the day-to-day variability) through data assimilation in IRI.

5. Conclusive remarks

This investigation highlighted how the assimilation of vTEC values calibrated by the *Seemala*'s and *Ciraolo*'s methods affects the updating of a background ionospheric model, in the specific case the IRI model. In other terms, the *IRI UP* method (Pignalberi et al, 2018a,b, 2019; Pignalberi, 2019) leads to important differences in the *fo*F2 modeling when the assimilated vTEC values are derived either from the *Ciraolo*'s calibration method (*IRI UP Ciraolo*) or from the *Seemala*'s calibration method (*IRI UP Seemala*). A first indication of that comes out from the comparison between the matrices shown in Fig. 3, where a significant improvement in the *fo*F2 modeling at nighttime hours and at the passage of solar terminator is observed in favour of *IRI UP Ciraolo*.

A detailed investigation of the whole analysis highlights without any doubt that the *IRI UP* method models *fo*F2 with a very good precision when the assimilated vTEC data are calibrated with the *Ciraolo*'s method. In this case, significant improvements are observed during nighttime hours and at solar terminator hours, while limited improvements are obtained during daytime hours. For what concerns the accuracy, it is not possible to define a vTEC calibration method better than the other.

This investigation revealed that the two calibration methods provide different vTEC values whose assimilation in *IRI UP* leads to output different *fo*F2 values, thus producing different results in terms of both precision and accuracy. This means that the reliability of vTEC time series to be assimilated plays a crucial role in achieving a precise and accurate *fo*F2 modeling.

For the future, the possibility to rely on a number of GNSS receivers over the European middle latitude region much larger than the one from the TrigNet network, it would allow to exploit the potentiality of the *IRI UP* method to achieve a reliable Space Weather nowcasting tool for the European area.

Declaration of Competing Interest

The authors declare that they have no known competing financial interests or personal relationships that could have appeared to influence the work reported in this paper.

Acknowledgments

This investigation uses data from four ionospheric observatories in South Africa, made available via the public access portal of the Digital Ionogram Database (http://ulcar.uml.edu/DIDBase/) of the Global Ionosphere Radio Observatory in Lowell, MA. Thanks to the TrigNet team for providing and making freely available GNSS data via the FTP access (ftp://ftp.trignet.co.za) and for its huge efforts in setting, maintaining, and developing its GNSS stations network. The IRI team is acknowledged for developing and maintaining the IRI model and for giving access to the corresponding Fortran code via the IRI website (http://irimodel.org/). Geomagnetic indices were downloaded from the OMNIWeb Data Explorer NASA site (https://omniweb.gsfc.nasa.gov/form/dx1.html). The authors would like also to thank Dr. Gopi Seemala for making freely available the software for the calibration of vTEC data (http://seemala.blogspot.com) and Dr. Luigi Ciraolo for providing us a tailored version of his calibration software. We wish to thank both reviewers for the useful and important comments they made. Their comments improved the manuscript clarity and soundness. A. Pignalberi is partially supported by the Italian MIUR-PRIN grant 2017APKP7T on Circumterrestrial Environment: Impact of Sun-Earth Interaction.

Appendix A. Supplementary material

Supplementary data to this article can be found online at https://doi.org/10.1016/j.asr.2020.10.040.

References

Arıkan, F., Sezen, U., Gulyaeva, T.L., 2019. Comparison of IRI-2016 F2 layer model parameters with ionosonde measurements. J. Geophys. Res. Space Phys. 124, 8092–8109. https://doi.org/10.1029/2019JA027048.

Bibl, K., Reinisch, B.W., 1978. The universal digital ionosonde. Radio Sci. 13, 519–530. https://doi.org/10.1029/RS013i003p00519.

Bilitza, D., Altadill, D., Truhlik, V., Shubin, V., Galkin, I., Reinisch, B. W., Huang, X., 2017. International Reference Ionosphere 2016: From ionospheric climate to real-time weather predictions. Space Weather 15, 418–429. https://doi.org/10.1002/2016SW001593.

Blagoveshchenskya, D.V., Sergeeva, M.A., 2019. Impact of geomagnetic storm of September 7–8, 2017 on ionosphereand HF propagation: a multi-instrument study. Adv. Space Res. 63 (1), 239–256. https://doi.org/10.1016/j.asr.2018.07.016.

Chi, P.J., Russell, C.T., Musman, S., Peterson, W.K., Le, G., Angelopoulos, V., et al., 2000. Plasmaspheric depletion and refilling associated with the September 25, 1998 magnetic storm observed by ground magnetometers at L = 2. Geophys. Res. Lett. 27 (5), 633–636. https://doi.org/10.1029/1999GL010722.

Ciraolo, L., Azpilicueta, F., Brunini, C., Meza, A., Radicella, S.M., 2007. Calibration errors on experimental slant total electron content (TEC) determined with GPS. J. Geod. 81 (2), 111–120. https://doi.org/10.1007/s00190-006-0093-1.

Davies, K., 1990. Ionospheric Radio. Peter Peregrinus Ltd., London, United Kingdom.

de Paula, E.R., de Oliveira, C.B.A., Caton, R.G., et al., 2019. Ionospheric irregularity behavior during the September 6–10, 2017 magnetic storm over Brazilian equatorial–low latitudes. Earth Planets Space 71, 42. https://doi.org/10.1186/s40623-019-1020-z.

Förster, M., Jakowski, N., 2000. Geomagnetic storm effects on the topside ionosphere and plasmasphere: a compact tutorial and new results. Surv. Geophys. 21 (1), 47–87. https://doi.org/10.1023/A:1006775125220.

Galkin, I.A., Reinisch, B.W., 2008. The new ARTIST 5 for all digisondes. Ionosonde Network Advisory Group Bulletin 69, 8 pp. (Available at: https://www.sws.bom.gov.au/IPSHosted/INAG/web-69/2008/artist5-inag.pdf).

Gerzen, T., Jakowski, N., Wilken, V., Hoque, M.M., 2013. Reconstruction of F2 layer peak electron density based on operational vertical total electron content maps. Ann. Geophys. 31, 1241–1249. https://doi.org/10.5194/angeo-31-1241-2013.

Liu, R.Y., Smith, P.A., King, J.W., 1983. A new solar index which leads to improved foF2 predictions using the CCIR Atlas. Telecommun. J. 50, 408–414.

Liu, Y., Li, Z., Fu, L., et al., 2020. Studying the ionospheric responses induced by a geomagnetic storm in September 2017 with multiple observations in America. GPS Solutions 24, 3. https://doi.org/10.1007/s10291-019-0916-1.

Kitanidis, P.K., 1997. Introduction to geostatistics: Application to hydrogeology. Cambridge University Press, Cambridge.

Klimenko, M.V., Klimenko, V.V., Zakharenkova, I.E., Cherniak, I.V., 2015. The global morphology of the plasmaspheric electron content during Northern winter 2009 based on GPS/COSMIC observation and GSM TIP model results. Adv. Space Res. 55 (8), 2077–2085. https://doi.org/10.1016/j.asr.2014.06.027.

Kouris, S.S., Xenos, T.D., Polimeris, K.V., Stergiou, D., 2004. TEC and *fo*F2 variations: preliminary results. Ann. Geophys. 47 (4), 1325–1332. https://doi.org/10.4401/ag-3346.

Krankowski, A., Shagimuratov, I.I., Baran, L.W., 2007. Mapping of foF2 over Europe based on GPS-derived TEC data. Adv. Space Res. 39 (5), 651–660. https://doi.org/10.1016/j.asr.2006.09.034.

Leitinger, L., Ciraolo, L., Kersley, L., Kouris, S.S., Spalla, P., 2004. Relations between electron content and peak density-regular and extreme behaviour. Ann. Geophysics 47 (2/3), 1093–1107. https://doi.org/10.4401/ag-3287.

Pezzopane, M., Del Corpo, A., Piersanti, M., et al., 2019. On some features characterizing the plasmasphere–magnetosphere–ionosphere system during the geomagnetic storm of 27 May 2017. Earth Planets Space 71, 77. https://doi.org/10.1186/s40623-019-1056-0.

Pietrella, M., Pignalberi, A., Pezzopane, M., Pignatelli, A., Azzarone, A., Rizzi, R., 2018. A comparative study of ionospheric IRIEup and ISP assimilative models during some intense and severe geomagnetic storms. Adv. Space Res. 61 (10), 2569–2584. https://doi.org/10.1016/j.asr.2018.02.026.

Pignalberi, A., Pezzopane, M., Rizzi, R., Galkin, I., 2018a. Effective solar indices for ionospheric modeling: a review and a proposal for a real-time regional IRI. Surv. Geophys. 39 (1), 125–167. https://doi.org/10.1007/s10712-017-9438-y.

Pignalberi, A., Pietrella, M., Pezzopane, M., Rizzi, R., 2018b. Improvements and validation of the IRI UP method under moderate, strong, and severe geomagnetic storms. Earth Planets Space 70, 180. https://doi.org/10.1186/s40623-018-0952-z.

Pignalberi, A., Habarulema, J.B., Pezzopane, M., Rizzi, R., 2019. On the development of a method for updating an empirical climatological ionospheric model by means of assimilated vTEC measurements from a GNSS receiver network. Space Weather 17, 1131–1164. https://doi.org/10.1029/2019SW002185.

Pignalberi, A., 2019. A three-dimensional regional assimilative model of the ionospheric electron density, PhD in Geophysics thesis, Alma Mater Studiorum Università di Bologna. doi: 10.6092/unibo/amsdottorato/8888, http://amsdottorato.unibo.it/8888/.

Reinisch, B.W., Galkin, I.A., 2011. Global ionospheric radio observatory (GIRO). Earth Planets Space 63 (4), 377–381. https://doi.org/10.5047/eps.2011.03.001.

Seemala, G.K., Valladares, C.E., 2011. Statistics of total electron content depletions observed over the South American continent for the year 2008. Radio Sci. 46, RS5019. https://doi.org/10.1029/2011RS004722.

Spalla, P., Ciraolo, L., 1994. TEC and *fo*F2 comparison. Annals of Geophysics 37 (5), 929–938. https://doi.org/10.4401/ag-3346.

Ssessanga, N., Mckinnell, L.A., Habarulema, J.B., 2014. Estimation of *fo*F2 from GPS TEC over the South African region. J. Atmos. Solar - Terrestrial Phys. 112, 20–30. https://doi.org/10.1016/j.jastp.2014.02.003.